RSC Advances

ROYAL SOCIETY OF CHEMISTRY

www.rsc.org/advances

Journal Name

ARTICLE

A new type acetylene gas sensor based on hollow heterostructure

Ying Lin [a], Chao Li [a], Wei Wei [a], Yujia Li [b], Shanpeng Wen [a, *], Dongming Sun [a], Yu Chen[c, *], Shengping Ruan [b,*]

A new type acetylene gas sensor based on the hollow NiO/SnO_2 heterostructure synthesized by two-step hydrothermal method and the followed-by calcination was fabricated. The properties of the sensing material were characterized by X-Ray diffraction (XRD), Scanning electron microscopy (SEM), energy-dispersive X-ray spectroscopy (EDX), Brunauer–Emmett–Teller (BET) and transmission electron microscopy (TEM). The acetylene gas-sensing performances were investigated. Compared with the pure SnO_2 gas sensor, the response of the hollow NiO/SnO_2 heterostructure gas sensor to 100 ppm acetylene (C_2H_2) was raised to 13.8 from 5.4 at the optimum operating temperature of 206 °C. A wide detection range from 1 – 1000 ppm and a low minimum detection limit of 1 ppm were obtained. In addition, the hollow NiO/SnO_2 heterostructure gas sensor had a good repeatability, selectivity, stability and rapid response-recovery characteristics.

Introduction

Various oxide semiconductor based gas sensors have been used to detect harmful and toxic gases. The most representative sensor materials are SnO_2 [1], ZnO [2], In_2O_3 [3-5], Fe_2O_3 [6], WO_3 [7], Co_3O_4 [8], TiO_2 [9], NiO, etc. In particular, SnO_2 has been widely used in gas sensor due to its high conductivity and good stability. To date, SnO_2 materials with different sizes and morphologies have been successfully synthesized, including nanowires [10], nanorods [11], nanofibers [12], nanobelts [13], nanotubes [2], etc. Moreover, the hollow structure has attracted much attention due to its low mass density, high surface area and tailored structure with less agglomerated configuration [14]. The hollow interior not only increases the surface area of the material, but also gives rise to the properties resulting from the electron distribution on the surface of the novel structure [15]. It can lead to an improved sensing performance in contrast to a conventional solid structured device.

Gas sensor is generally characterized by its response, response-recovery time and selectivity, among which the response weighs a lot because a higher response usually means a significant ability for gas detection at lower concentration level. Therefore, many efforts have been concentrated on the improvement of response towards different gases. After continuous researches, it is found that the heterostructure can effectively improve the gas sensing performance. The p–n junction between oxide semiconductor materials can also be used to alter the gas-sensing characteristics of gas sensors by varying the electrical properties near heterointerfaces [16, 17]. On the other hand, the sensing performances are also dependent on the gases. At present, many gas sensors with high properties have been obtained in detecting CH_3CH_2OH [18, 19], CH_3COCH_3 [7, 12], HCHO [20, 21], CO [22, 23], NO_2 [24, 25], etc. However, the researches on the acetylene (C_2H_2) are not enough. Acetylene is the most effective and versatile fuel gas, enabling manual applications in welding, cutting, straightening, and other localized heating process. Moreover, acetylene is a kind of colorless and odorless gas which is not easy to detect in the air and highly combustible and explosive. Therefore, great efforts are required to fabricate practical acetylene sensor.

In this work, the hollow NiO/SnO_2 heterostructure was successfully synthesized by two-step hydrothermal method and the followed-by calcination. Their acetylene sensing properties of the sensors were examined. Compared with the pure SnO_2 gas sensor, the response of hollow NiO/SnO_2 heterostructure gas sensor was enhanced from 5.4 to 13.8, and the response-recovery time was 2 s and 5s, which was much faster than most reported articles. The possible mechanism about the effects on the acetylene sensing properties induced by the hollow structure and the heterostructure was discussed.

Experimental

Chemical reagent

All the starting materials (AR grade): Glucose $(C_6H_{12}O_6)$, Urea $(CO(NH_2)_2)$, Nickel chloride $(NiCl_2·6H_2O)$, Tin(Ⅱ) chloride dehydrate $(SnCl_2·2H_2O)$, 1,2-Propanediol $(CH_3CH(OH)CH_2OH)$,
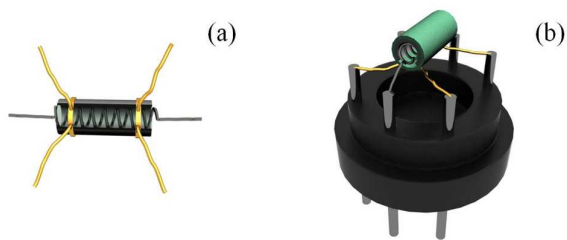
Fig. 1(a) the section image of the ceramic tube; (b) the schematic image of the sensor

Ammonia solution (25%) (NH$_3$·H$_2$O) and Hydrogen peroxide (H$_2$O$_2$) were purchased from the Sinopharm Chemical Reagent Co. Ltd. and used as received without any further purification.

Synthesis process

Firstly, NiO nanocubes were synthesized by the hydrolysis of Nickel salt. Briefly, NiCl$_2$·6H$_2$O (0.3 g), C$_6$H$_{12}$O$_6$ (0.448 g) and CO(NH$_2$)$_2$ (0.5 g) were dissolved in 30 mL distilled water. Then the mixture was poured into a Teflon lined stainless steel autoclave and heated at 200 °C for 10 h. After centrifugation, washing and drying, NiO nanocubes were collected. Secondly, the NiO/SnO$_2$ heterostructure was prepared by a hydrothermal method. In a typical procedure, 0.05 g of the as-prepared NiO nanocubes were dispersed in a mixture of 1,2-propanediol (30 mL), distilled water (30 mL), and ammonia solution (4 mL). Subsequently, H$_2$O$_2$ (2 mL) and SnCl$_2$·2H$_2$O (0.45 g) were introduced. After stirring for 15 min, the solution was transferred into a Teflon-lined stainless steel autoclave, and maintained at 120 °C for 15 h and then cooled down to room temperature naturally. The products were washed several times with distilled water and ethanol, and finally dried in a vacuum oven at 60 °C for 12 h. In the end, the hollow NiO/SnO$_2$ heterostructure was obtained after the above products were annealed. At the same time, the pure SnO$_2$ material was synthesized in the same ambient. SnCl$_2$·2H$_2$O (0.45 g) was added in 1,2-propanediol (30 mL), distilled water (30 mL), ammonia solution (4 mL) and H$_2$O$_2$ (2 mL). After the hydrothermal process and calcinations, the pure SnO$_2$ material was collected for later use.

Characterization

X-Ray diffraction (XRD) analysis was conducted on a Scintag XDS-2000 X-ray diffractometer with Cu Kα radiation (λ=1.5418 Å). Scanning electron microscopy (SEM) images were performed on a SHIMADZU SSX-550 (Japan) instrument. Energy-dispersive X-ray spectroscopy (EDX) was obtained on a JEM-ARM200F microscope. Transmission electron microscopy (TEM) images were obtained using a TECNAI G2 electron microscope. Surface area and pore size distribution were evaluated using Brunauer–Emmett–Teller (BET) and Barrett–Joyner–Halenda (BJH) methods, respectively.
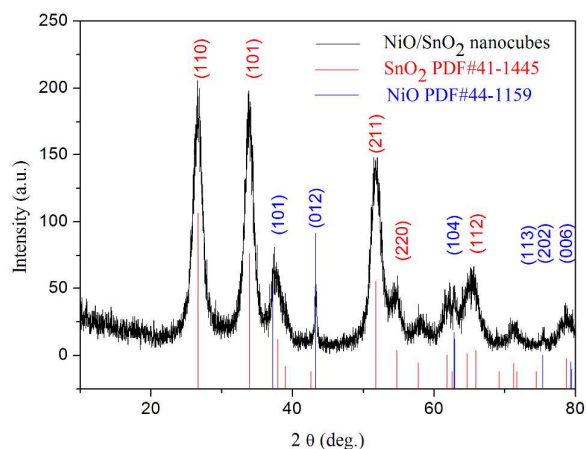
Fig. 2 XRD patterns of hollow NiO/SnO$_2$ heterostructure.

Fabrication and measurement of gas sensor

Sensor device was fabricated by similar method in our previous works [26, 27]. The as-prepared samples were mixed with deionized water in a weight ratio of 4:1 and ground in a mortar to form a paste. Then the paste was coated on a ceramic tube as a sensing film with a thickness of about 300 μm. After the ceramic tube was calcined at 300 °C for 2 h, a Ni-Cr heating wire was inserted in the tube as a heater for controlling the operating temperature. The section image of the ceramic tube and the schematic image of the sensor were shown in Fig. 1.

Gas sensing properties were measured by a chemical gas sensor-8 (CGS-8) intelligent gas sensing analysis system (Beijing Elite Tech Co. Ltd., China) under room condition (25 °C, 40 RH%). All the sensors were pre-heated at different operating temperatures for about 30 min. When the resistances of the sensors were stable, the target gas was injected into the test chamber (20 L in volume) by a microinjector through a rubber plug. The saturated target gas was mixed with air (relative humidity was about 40%, which was measured by a humidity sensor) by two fans in the analysis system. After the sensor resistances reached a new constant value, the test chamber was opened to recover the sensors in air. All the measurements were performed in a laboratory fume hood in a super-clean room. After the sensor resistances reached new constant value, the sensor was moved out of the target gas and put it in the air until the sensor restored the stable value. The response of the sensor to reducing gas was defined as R_a/R_g and to oxidizing gas was defined as R_g/R_a, where Ra and R_g were the resistances in air and test gas, individually. The time taken by the sensor' to achieve 90% of the total resistance change was defined as the response time in the case of target gas adsorption or the recovery time in the case of target gas desorption.

Results and discussion
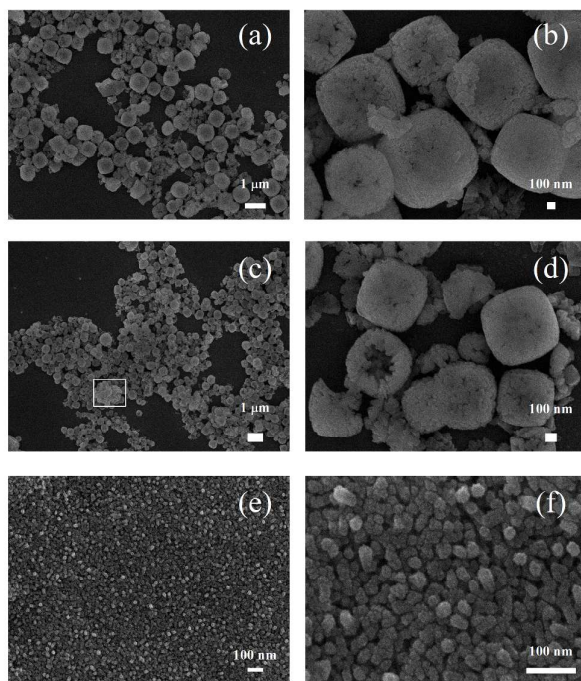
Fig.3. Low (a) and high (b) magnification SEM images of NiO/SnO$_2$ heterostructure calcined at 600°C; low (c) and high (d) magnification SEM images of NiO/SnO$_2$ heterostructure calcined at 700°C; Low (e) and high (f) magnification SEM images of pure SnO$_2$ calcined at 600°C.

Structural and morphological characteristics

The XRD patterns of NiO prepared by the first hydrothermal method were exhibited in Fig. S1. The peaks appeared at 37.28°, 43.28°, 62.88°, 75.4°, 79.4° and 79.46° were corresponding to (101), (012), (104), (113), (202) and (006), respectively, crystal planes of the nickel oxide (JCPDS card no. 44-1159). And Fig.2 showed the XRD patterns of as-prepared samples. Most of the diffraction peaks can be readily indexed to the tetragonal phase tin oxide, which were well agreed with the reported values from the Joint Committee on Powder Diffraction Standards Card (JCPDS card no. 41-1445). Furthermore, some peaks appeared at 37.28°, 43.28°, 62.88°, 75.4°, 79.4° and 79.46° were corresponding to NiO as shown in Fig. S1. It indicated the existence of SnO$_2$ and NiO in the NiO/SnO$_2$ heterostructure. From the XRD peaks, the lattice parameters of the SnO$_2$ and NiO in the hollow NiO/SnO$_2$ heterostructure were about 6.7 nm and 24.6 nm, respectively.

The NiO/SnO$_2$ heterostructure was prepared by two-step hydrothermal method. The SEM image of the NiO nanocubes with the diameter of 800 nm was shown in Fig. S2. Then SnO$_2$ was grown outside of the NiO nanocubes by the second hydrothermal process. After calcinations the hollow NiO/SnO$_2$ heterostructure was successfully synthesized. The reason of the formation of the hollow structure was as follows: In the first hydrothermal process the glucose reacted and came into
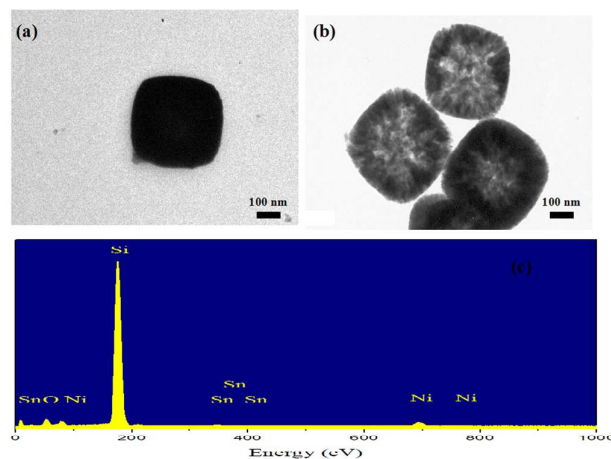
Fig. 4. TEM images of NiO/SnO$_2$ heterostructure (a) before calcinations; (b) after calcination; (c) EDX spectra of NiO/SnO$_2$ heterostructure.

being carbon. After calcinations, the carbon reacted with the oxygen in the air and turned into carbon dioxide which left the vacancy and grew the hollow structure.

Fig. 3 showed the low and high magnification SEM images of NiO/SnO$_2$ heterostructure calcined at 600 °C and 700 °C, respectively. After calcined at 600 °C as shown in Fig. 3(a) and (b), the homogeneous NiO/SnO$_2$ nanocubes with the diameter of about 900 nm were prepared. While calcined at 700 °C as shown in Fig. 3(c) and (d), the homogeneity was not as good as calcined at 600 °C. Some nanocubes were incomplete and appeared the reunion phenomenon. Therefore, 600 °C was the optimal calcination temperature of hollow NiO/SnO$_2$ heterostructure. In addition, the SEM images of pure SnO$_2$ were shown in Fig. 3(e) and (f). It can be seen that the pure SnO$_2$ was composite of uniform nanoparticles with a diameter of about 30 nm.

To further confirm the NiO/SnO$_2$ heterostructure was hollow, TEM characterization was conducted. Fig. 4(a) and (b) were the TEM images before and after calcinations, respectively. Fig. 4(a) clearly demonstrated the solid structure of the as-prepared NiO/SnO$_2$ heterostructure before calcinations. After calcinations the hollow structure was obtained as shown in Fig. 4(b). The formation of the hollow structure was mainly due to the carbon in the materials transformed into carbon dioxide and left the vacancy. While the TEM image of pure SnO$_2$ was
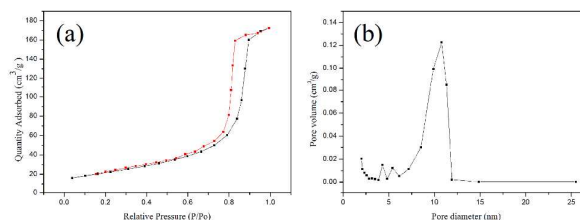
Fig. 5. (a) Typical N$_2$ adsorption–desorption isotherms and (b) pore-size distribution curve of hollow NiO/SnO$_2$ composite.

COMMUNICATION

provided in Fig. S3 which exhibited the pure SnO_2 was not the hollow structure. The corresponding EDX was exhibited in Fig. 4(c) which revealed that the as-prepared material consisted of O, Sn and Ni elements. Besides, the Si element signal in the spectrum was attributed to the SEM grid used to support the sample. Fig. S4 showed the EDX mapping of all elements in the hollow NiO/SnO_2 heterostructure. It could be seen that O, Sn and Ni were quiet evenly distributed over the area. Therefore, it is reasonable to believe that SnO_2 was wrapped on the surface of NiO nanocubes. Furthermore, the corresponding atom ratio of SnO_2 and NiO was 3:11 in the composite.

The BET specific surface area was investigated by using nitrogen adsorption and desorption isotherms. Fig. 5 showed the nitrogen adsorption-desorption isotherms of the hollow NiO/SnO_2 composite. The BET specific surface areas of the hollow NiO/SnO_2 composite and pure SnO_2 were 75.86750 $m^2 \cdot g^{-1}$ and 21.03852 $m^2 \cdot g^{-1}$, respectively. The specific surface area of hollow NiO/SnO_2 composite is much higher than that of the pure SnO_2, and it will be an advantage to improve the gas-sensing properties. The pore-size distribution (Fig. 5(b)) was determined by using the BJH method from the desorption branch of the isotherm, the average pore diameter of the

hollow NiO/SnO_2 composite was about 9.09638 nm.

Gas sensor performance

In order to determine the optimum operating temperature, the responses of the hollow NiO/SnO_2 gas sensor and pure SnO_2 gas sensor to 100 ppm acetylene vapor were measured continually at different operating temperatures. Fig. 6 showed the response as a function of operating temperature from 50 to 300 °C. As the operating temperature increased, the responses of the hollow NiO/SnO_2 gas sensors increased at first and reached the maximum value at 206 °C, followed by a decrease gradually. The pure SnO_2 gas sensor reached the maximum response at 206 °C, too. In addition, the corresponding relation between resistance and the operating temperature was shown in Fig. S5. Therefore, 206 °C was the optimal operating temperature of the hollow NiO/SnO_2 gas sensor and pure SnO_2 gas sensor. The following studies about the sensors' acetylene sensing properties were operated at the optimal operating temperature.

Fig. 7 shows the typical response curves of the hollow NiO/SnO_2 gas sensor and the pure SnO_2 gas sensor with an
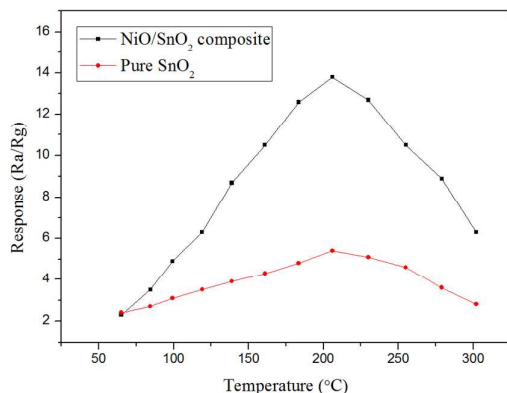
Fig. 6. The sensors' responses to 100 ppm acetylene at different operating temperatures.
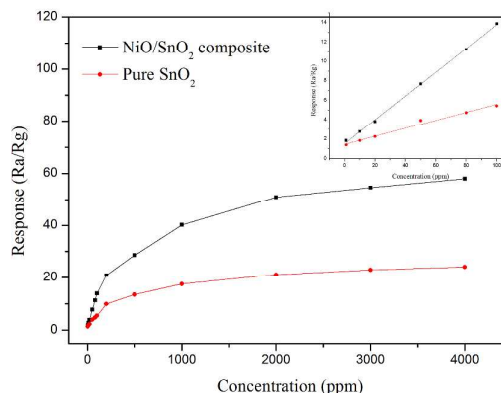
Fig. 7. Curves of sensors' responses versus acetylene concentrations at their optimum operating temperature.
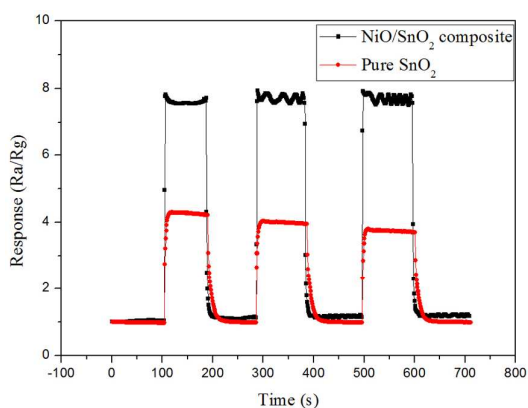
Fig. 8. Repeatability of the sensors to 50 ppm acetylene at their optimum operating temperature.
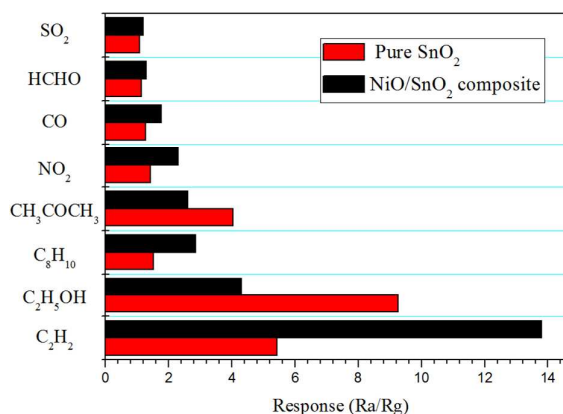
Fig. 9. Responses of the sensors to 100 ppm different gases at their optimum operating temperature.

Material	Method	Temperature (°C)	Response	Detection limit (ppm)	Res-rev time (s)	Ref.
Pt/ZnO	Flame spray pyrolysis	300	1.1 (50ppm)	50	6/65	[28]
Sm_2O_3-SnO_2	Sol gel	180	8.3 (100ppm)	50	3/17	[29]
SnO_2	Spin coating	300	6.3 (10000ppm)	200	34/>10min	[30]
Ni-ZnO	Electrospinning	250	6 (500ppm)	100	5/10	[31]
Ag-ZnO	Photochemical	200	13 (100ppm)	5	57/90	[32]
NiO/SnO_2	Hydrothermal	206	13.8 (100ppm)	1	2/5	This work

Table 1. Various metal oxide semiconductor gas sensors to acetylene surveyed in literatures.

increasing concentration of acetylene at 206 °C. It can be easily found that the responses increased rapidly with the acetylene concentration (1-100 ppm), and then gradually slowed down (100-1000 ppm), which indicated the sensor became gradually saturated. Finally the sensor reached saturation above 1000 ppm. The response of hollow NiO/SnO_2 gas sensor was much higher than the pure SnO_2 gas sensor in the full concentration range. Moreover, the insert in Fig. 7 shows the linear calibration curve of both the sensors in the range of 1-100 ppm. It was obvious that the hollow NiO/SnO_2 gas sensor had a better linear calibration curve than the pure SnO_2 gas sensor. In other words, the hollow NiO/SnO_2 gas sensor owned better acetylene properties. Moreover, the minimum detection limit of the hollow NiO/SnO_2 gas sensor was 1 ppm, and the corresponding response was about 1.8. The low minimum detection limit and the excellent linear dependence further showed that the hollow NiO/SnO_2 gas sensor can be used as promising materials of acetylene sensors.

For testing the repeatability of the sensors, the same device was tested three times continuously to 50 ppm acetylene at their optimal operating temperatures. The corresponding result was shown in Fig. 8. It could be seen that the hollow NiO/SnO_2 gas sensor had the paralleled gas sensing properties among the three times which demonstrated a good repeatability. While the response value of the pure SnO_2 gas sensor was decreased in the continuous testing. Compared with the pure SnO_2 gas sensor, the hollow NiO/SnO_2 gas sensor had a better stability and could be monitored continuously. Furthermore, the response and recovery time of the hollow NiO/SnO_2 gas sensor were about 2 s and 5 s, which were better than the pure SnO_2 gas sensor of 6 s and 15 s, respectively. The remarkably shorter response-recovery time can be attributed to the hollow structure, which provided larger active surface area and accelerated diffusion [21]. The response-recovery curves in the range of 1-5000 ppm concentrations of acetylene were exhibited in the Fig. S6.

The gas sensing selectivity is another important parameter to evaluate the sensing ability of semiconductor materials. The selectivity of hollow NiO/SnO_2 gas sensor and the pure SnO_2 gas sensor were tested by exposing the sensor to 100 ppm potential interference gases such as ethanol (EtOH), acetone (CH_3COCH_3), nitrogen dioxide (NO_2), sulfur dioxide (SO_2), formaldehyde (HCHO) and so on. From Fig. 9, it can be seen

that the hollow NiO/SnO_2 gas sensor exhibited an obvious response to acetylene and less effect to other gases at 206 °C. It illustrates that the hollow NiO/SnO_2 gas sensor has a good selectivity to acetylene.

Fig. S7 displayed the stability of the hollow NiO/SnO_2 gas sensor which was measured to 50ppm acetylene at 206 °C for 30 days. In the experiments, the sensor was tested every two days. The results exhibited that the response changed little during the times. It was obvious that the sensor based on the hollow NiO/SnO_2 gas sensor had a good stability which could be put into various practical applications. In addition, in Table 1, the sensing performances of hollow NiO/SnO_2 gas sensor were compared with the sensors fabricated from various materials in terms of acetylene sensing capabilities [28-32]. It can be seen that the sensor based on the hollow NiO/SnO_2 heterostructure had a low operating temperature, low minimum detection limit, high response and rapid response-recovery characteristics.

Gas sensing mechanism

SnO_2 is one of the most representative n-type oxide semiconductor gas sensing materials and its sensing mechanism is explained as the change in electrical conductivity caused by the chemical interaction of gas molecules with the surface of the semiconductor metal oxides [16]. In air ambient, the oxygen will capture electrons from SnO_2 conduction band to generate ions in the form of O_2^- (ads), O^-(ads) or O^{2-}(ads). It will result in an electron depletion layer which enlarges electron transport barrier between particles. In acetylene ambient, the reducing molecules will react with the adsorbed oxygen ions and release the trapped electrons back to SnO_2 conduction band, leading to a reduced electron depletion barrier and contracted electron transport barrier. The following reaction may take place [33]:

$$C_2H_2 + 5\ O^-_{(ads)} \rightarrow 2CO_2 + H_2O + 5\ e^-$$
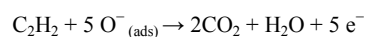
For NiO/SnO_2 composite's situation, as shown in Fig. 10(c) and (d), the corresponding acetylene-sensing process is similar to that of individual SnO_2 mentioned above. In order to clarify the good gas-sensing performance, a possible response mechanism is offered, as presented in Fig. 10. On the one hand,

the heterojunction is considered as an important reason for the dramatically enhanced sensitivity of heterostructure materials [20, 34]. As we all know that SnO_2 is a kind of n-type oxide semiconductor with a wide band gap of 3.6 eV, and NiO is one typical p-type oxide semiconductor with a wide band gap of 3.9 eV [34]. At the interface between NiO and and SnO_2 nanoparticles many p–n junctions are generated [35]. The electrons transform from n-type SnO_2 to p–type NiO while the holes transform from p–type NiO to n-type SnO_2 until the system obtains equalization at the Fermi level, the wide depletion regions are generated leading to a remarkable decrease in conductivity. When the sensor based on the NiO/SnO_2 heterostructure is exposed to acetylene ambient, the electrons trapped by absorbed oxygen species and NiO nanoparticles are feed back to SnO_2 through surface interactions, which will shrink p-n junction depletion regions and decrease the barrier height. As a result, the conducting channel will be widened and the conductivity could increase significantly. Therefore, the sensor response is remarkably improved [36, 37].

On the other hand, compared with the solid structure, the hollow structure has more surface area (inner and outer) which makes the molecules adsorb on the surfaces easily [38]. Additionally, the gas molecules could freely pass into and out of the SnO_2 materials and provides more gas channels [39]. Then the gas transform properties are improved. After the reducing gas reacts with the oxygen species, the electron concentration is increased [40]. The hollow structures facilitate the transfer of the acetylene molecules as well as improve the rate of the charge carriers to traverse the barriers [41]. As a consequence, a high response is obtained.

Conclusions

In conclusion, the hollow NiO/SnO_2 heterostructure were successfully synthesized by two-step hydrothermal method and the followed-by calcination. Compared with the pure SnO_2 gas sensor, the hollow NiO/SnO_2 gas sensor had better acetylene sensing properties, such as a high response (13.8 to 100 ppm acetylene), low minimum detection limit (1 ppm), rapid response/recovery characteristics (2 s and 5 s, respectively), a good repeatability, selectivity and stability. Based on the above reasons it is advisable that the hollow NiO/SnO_2 gas sensor is a promising candidate for a good performance acetylene sensor.

Acknowledgements

Notes and references

[a] State Key Laboratory on Integrated Optoelectronics, Jilin University, Changchun 130012, P. R. China. *Email:* sp_wen@jlu.edu.cn
[b] College of Electronic Science and Engineering, Jilin University, Changchun 130012, P. R. China. *Email: ruansp@jlu.edu.cn*
[c] Institute of Semiconductors, Chinese Academy of Sciences, Beijing 100083, China. *Email:* chenyu_1099@163.com (Y.Chen)

†Electronic Supplementary Information (ESI) available: See DOI: 10.1039/b000000x/

1. L. M. Fang, X. T. Zu, Z. J. Li, S. Zhu, C. M. Liu, L. M. Wang and F. Gao, *Journal of Materials Science: Materials in Electronics*, 2008, **19**, 868-874.
2. S. Cho, D.-H. Kim, B.-S. Lee, J. Jung, J.-W. Yu, S.-H. Hong and S. Lee, *Sensors and Actuators B: Chemical*, 2012, **162**, 300-306.
3. S. K. Lim, S.-H. Hwang, D. Chang and S. Kim, *Sensors and Actuators B: Chemical*, 2010, **149**, 28-33.
4. Hafeezullah, Z. H. Yamani, J. Iqbal, A. Qurashi and A. Hakeem, *J Alloys Compd*, 2014, **616**, 76-80.
5. Y. Wang, B. Liu, D. Cai, H. Li, Y. Liu, D. Wang, L. Wang, Q. Li and T. Wang, *Sensors and Actuators B: Chemical*, 2014, **201**, 351-359.
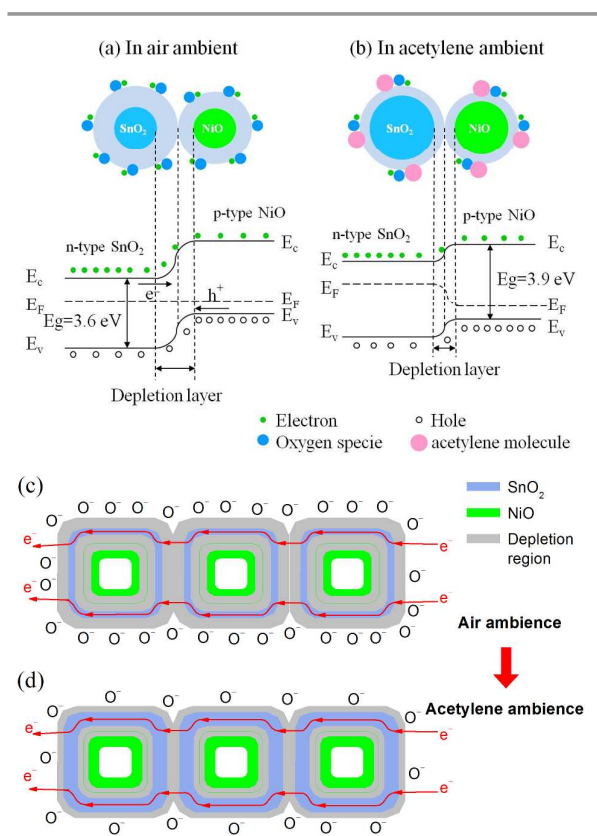
Fig. 10. Mechanism diagram of hollow NiO/SnO_2 heterostructure to acetylene.

COMMUNICATION

6. S. T. Navale, G. D. Khuspe, M. A. Chougule and V. B. Patil, *Organic Electronics*, 2014, **15**, 2159-2167.

7. T. Xiao, X.-Y. Wang, Z.-H. Zhao, L. Li, L. Zhang, H.-C. Yao, J.-S. Wang and Z.-J. Li, *Sensors and Actuators B: Chemical*, 2014, **199**, 210-219.

8. B. Geng, F. Zhan, C. Fang and N. Yu, *Journal of Materials Chemistry*, 2008, **18**, 4977-4984.

9. E. Sennik, N. Kilinc and Z. Z. Ozturk, *J Alloys Compd*, 2014, **616**, 89-96.

10. J. Guo, J. Zhang, M. Zhu, D. Ju, H. Xu and B. Cao, *Sensors and Actuators B: Chemical*, 2014, **199**, 339-345.

11. A. Khayatian, M. A. Kashi, R. Azimirad and S. Safa, *J Phys D Appl Phys*, 2014, **47**, 075003.

12. S. Wei, M. Zhou and W. Du, *Sensors and Actuators B: Chemical*, 2011, **160**, 753-759.

13. M. Amin, N. A. Shah, A. S. Bhatti and M. A. Malik, *CrystEngComm*, 2014, **16**, 6080-6088.

14. F. Dong, W. Guo, S.-S. Park and C.-S. Ha, *Journal of Materials Chemistry*, 2011, **21**, 10744.

15. R. Gao, S. Zhou, M. Chen and L. Wu, *Journal of Materials Chemistry*, 2011, **21**, 17087.

16. H.-J. Kim and J.-H. Lee, *Sensors and Actuators B: Chemical*, 2014, **192**, 607-627.

17. Z. L. Zhaojie Wang, Jinghui Sun, Hongnan Zhang, Wei Wang, Wei Zheng, and Ce Wang,, *J. Phys. Chem. C*, 2010, **114**, 6100–6105.

18. C. Feng, W. Li, C. Li, L. Zhu, H. Zhang, Y. Zhang, S. Ruan, W. Chen and L. Yu, *Sensors and Actuators B: Chemical*, 2012, **166-167**, 83-88.

19. D. Ju, H. Xu, J. Zhang, J. Guo and B. Cao, *Sensors and Actuators B: Chemical*, 2014, **201**, 444-451.

20. H. Du, J. Wang, M. Su, P. Yao, Y. Zheng and N. Yu, *Sensors and Actuators B: Chemical*, 2012, **166-167**, 746-752.

21. L. Wang, X. Luo, X. Zheng, R. Wang and T. Zhang, *RSC Advances*, 2013, **3**, 9723.

22. D. Patil, P. Patil, V. Subramanian, P. A. Joy and H. S. Potdar, *Talanta*, 2010, **81**, 37-43.

23. C.-M. Chang, M.-H. Hon and I.-C. Leu, *RSC Advances*, 2012, **2**, 2469.

24. J. Kaur, S. C. Roy and M. C. Bhatnagar, *Sensors and Actuators B: Chemical*, 2007, **123**, 1090-1095.

25. J. Kaur, V. D. Vankar and M. C. Bhatnagar, *Sensors and Actuators B: Chemical*, 2008, **133**, 650-655.

26. Y. Lin, Y. Wang, W. Wei, L. Zhu, S. Wen and S. Ruan, *Ceramics International*, 2015, **41**, 7329-7336.

27. Y. Chen, L. Zhu, C. Feng, J. Liu, C. Li, S. Wen and S. Ruan, *J Alloys Compd*, 2013, **581**, 653-658.

28. N. Tamaekong, C. Liewhiran, A. Wisitsoraat and S. Phanichphant, *Sensors and Actuators B: Chemical*, 2011, **152**, 155-161.

29. Q. Qi, T. Zhang, X. Zheng, H. Fan, L. Liu, R. Wang and Y. Zeng, *Sensors and Actuators B: Chemical*, 2008, **134**, 36-42.

30. C. Liewhiran, N. Tamaekong, A. Wisitsoraat and S. Phanichphant, *Sensors and Actuators B: Chemical*, 2012, **163**, 51-60.

31. X. Wang, M. Zhao, F. Liu, J. Jia, X. Li and L. Cao, *Ceramics International*, 2013, **39**, 2883-2887.

32. A. S. M. Iftekhar Uddin, K.-W. Lee and G.-S. Chung, *Sensors and Actuators B: Chemical*, 2015, **216**, 33-40.

33. P. Hu, N. Han, D. Zhang, J. C. Ho and Y. Chen, *Sensors and Actuators B: Chemical*, 2012, **169**, 74-80.

34. Y. Chen, L. Yu, D. Feng, M. Zhuo, M. Zhang, E. Zhang, Z. Xu, Q. Li and T. Wang, *Sensors and Actuators B: Chemical*, 2012, **166-167**, 61-67.

35. N. Wu, M. Zhao, J.-G. Zheng, C. Jiang, B. Myers, S. Li, M. Chyu and S. X. Mao, *Nanotechnology*, 2005, **16**, 2878-2881.

36. K. Adolfsson, H. Persson, J. Wallentin, S. Oredsson, L. Samuelson, J. O. Tegenfeldt, M. T. Borgstrom and C. N. Prinz, *Nano Lett*, 2013, **13**, 4728-4732.

37. Z. Lou, F. Li, J. Deng, L. Wang and T. Zhang, *ACS Appl Mater Interfaces*, 2013, **5**, 12310-12316.

38. M. Yin and S. Liu, *Sensors and Actuators B: Chemical*, 2014, **197**, 58-65.

39. J. Huang, L. Wang, C. Gu, M. Zhai and J. Liu, *CrystEngComm*, 2013, **15**, 7515-7521.

40. W. Q. Li, S. Y. Ma, J. Luo, Y. Z. Mao, L. Cheng, D. J. Gengzang, X. L. Xu and S. H. Yan, *Materials Letters*, 2014, **132**, 338-341.

41. Y. E. Chang, D. Y. Youn, G. Ankonina, D. J. Yang, H. G. Kim, A. Rothschild and I. D. Kim, *Chem Commun (Camb)*, 2009, 4019-4021.

Graphical Abstract
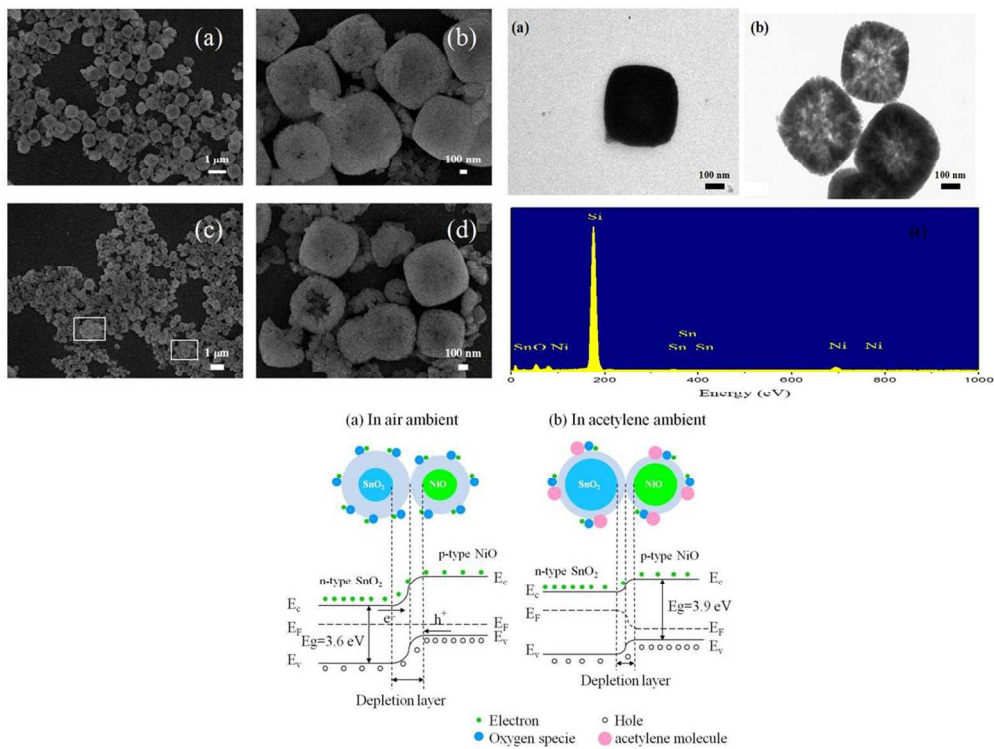
Text: The SEM, TEM and the mechanism images of hollow NiO/SnO_2 heterostructure.

217x183mm (150 x 150 DPI)